Int. J. Electrochem. Sci., 8 **(2013)** 10320 - 10334

International Journal of ELECTROCHEMICAL SCIENCE
www.electrochemsci.org

The Effect of Copper Alloying Element on the Corrosion Characteristics of Ti-Ni and Ternary Ni-Ti-Cu Meltspun Shape Memory Alloy Ribbons in 0.9% NaCl Solution

Corneliu Craciunescu[1] *and Abdel Salam Hamdy*[2]

[1] Department of Materials Science, "Politehnica" University of Timisoara, Bd. Mihai Viteazul 1, 1900 Timisoara, Romania
[2] Central Metallurgical Research and Development Institute, CMRDI, P. O. Box: 87, 11421 Cairo, Egypt
[*]E-mail: asalam85@yahoo.com

Received: 11 June 2013 / *Accepted:* 27 June 2013 / *Published:* 1 August 2013

This paper provides a new insight towards understanding the mechanism of corrosion of ternary Ni-Ti-Cu shape memory alloy ribbons manufactured by meltspinning in 0.9% NaCl solution. A new mechanism has been proposed to explain the pitting susceptibility and the role of copper on the Ni diffusion in Ti-Ni and Ti-Ni-Cu alloys. It has been evidenced that pitting is the most predominant corrosion form in Ti-Ni due to Ni dissolution. The presence of copper improved the resistance to pitting corrosion. Results showed that the most predominant corrosion form in Ti-Ni-Cu is general corrosion with some pits. The new findings will help the manufactures of shape memory alloys (SMAs) in designing materials of better durability and longer life time.

Keywords: shape memory alloys, rapid solidification, pitting corrosion, Ti-Ni-Cu.

1. INTRODUCTION

The characterization of corrosion and biocompatibility behavior of rapidly solidified materials finds increasing academic and industrial interests due to the expansion of the research in the amorphous and nanocrystalline range [1]. Higher corrosion resistance, reflected by a tendency to passivation and lower anodic current density than similar amorphous alloy was reported on Fe-based alloy [2]. The corrosion behavior of materials manufactured via different processes in the nanocrystalline range is especially important as potential materials to be used in biomedical applications [3,4]. Although the corrosion resistance of fully amorphous Ti-alloys is expected to be

better than the one in the fully crystalline form [5], recent studies showed an improved corrosion resistance for some alloys as the crystallization proceeds [6].

Shape memory alloys (SMAs) have been considered for some years for practical applications in various environments due to their capacity to recover the shape they had before a plastic deformation by simply heating above the critical temperature. Nitinol, the trade name for Ni-Ti, can be used in extreme environments due to a high corrosion resistance and/or due to its biocompatibility. The electrochemical corrosion behavior of Nitinol was a critical issue, especially if the passive film formed is not homogenous [7]. The addition of alloying elements is another important issue that can significantly influence the behavior of NiTi shape memory alloys in particular environments. Zheng et al. confirmed the positive effects of Ag addition on NiTi alloys [8] and Cr addition on TiNiCu alloys [9].

Among the alloying elements, copper appears to be an important one because it can shape the hysteresis and actuation characteristics. For Ti-Ni-Cu alloys, the replacement of Ni by Cu shifts the phase transition from a B2→ monoclinic one to a B2→ orthorhombic → monoclinic one [10]. Such alloys show interesting actuating properties as well as superelastic properties as bulk, ribbon [11,12] and free-standing [13], or attached to substrate thin films [14], leading to interesting applications [15]. Cu contents higher than 10% appear to produce embrittlement in bulk alloys, but the meltspinning process allows the increase of Cu content up to significant values [16]. It appears that increasing copper content may have a positive contribution to the repassivation potential of Ni-Ti based alloys, leading to an increased corrosion resistance. However, the work done by Wen et al [17] suggests that the corrosion rate is irrelevant to its Cu content when up to 8 % Cu is replacing Ni.

Varying the heating temperatures before meltspinning and cooling rates may lead to structures ranging from amorphous to crystalline [18] and similar amorphous–crystalline structures can be obtained by an interruption of the crystallization process [19]. It has been reported that depending on the heating temperature prior to meltspinning of such alloys, the resulting structure could be amorphous or amorphous with crystalline inclusions of B2 austenite phase [20]. Both structures can be converted to a crystalline form by proper annealing, and for $Ti_{50}Ni_{25}Cu_{25}$ ribbons the resulting transformation is a B2–B19 [21]. Amorphous shape memory alloys do not show the shape memory effect, which starts to develop only during the crystallization, as observed for Ni_2MnGa ferromagnetic shape memory alloys [22].

The formation of TiO_2 passive film on the surface is extremely important for improving the corrosion resistance of Nitinol, while releasing of Ni ions from Ni-Ti surface is the main reason of lowering corrosion resistance and biocompatibility. Rondeli and Vicentini [23] showed that Ni-Ti and $Ni_{44}Ti_{51}Cu_5$ exhibit low corrosion potential in 0.9% NaCl, in the range of 50-150 mV versus SCE. Bertacchini et al studied the corrosion-assisted fatigue of TiNiCu alloys and observed enhanced and accelerated damage mechanisms due to corrosion [24]. Other studies revealed that TiNiCu dissolves at low electrode potential (100 mV ∼ 150 mV) when it is anodically polarized, with pitting corrosion sensibility promoted for higher Cl^- concentration [25]. The effect of ternary element addition on the corrosion behavior of NiTi alloys has been investigated. The localized corrosion resistances has been sorted in the following order: NiTiCu < NiTiFe < NiTiPd < NiTi. The decrease in the localised

corrosion resistances was attributed to the ternary elements distributed in the TiO_2 layer for NiTiPd and NiTiCu alloys, whereas the NiTi-based alloys had mainly TiO_2 as surface oxide film [26]

It has recently been reported for $Ti_{50}Ni_{41}Cu_9$ thin films that the release of Ni and Cu ions is much less than the toxic level and the film did not lose shape memory effect even after 10-day immersion in simulated gastric and intestinal solutions [27].

The objective of the present study is to explore the corrosion behavior of as-spun Ti-Ni-Cu shape memory alloys at higher copper content in ribbons produced by meltspinning. This paper aims also to provide a better understanding about the mechanism of corrosion of ternary Ni-Ti-Cu shape memory alloy in 0.9% NaCl solution

2. EXPERIMENTAL

2.1. Materials:

The melt-spinning technique was used for manufacturing shape memory ribbons. Ribbons of 30 μm thickness and 2 mm width were produced by melt-spinning out of a master alloy with nominal composition $Ti_{50}Ni_{25}Cu_{25}$ (wt%) prepared by arc melting in high vacuum. The as-manufactured alloy was then melted in an induction furnace and melt-spun on the outer surface of a copper drum. The cooling rate was in the range of 10^{-6} K/s.

In order to investigate the corrosion behavior of Ti-Ni-Cu ribbons and compare with other shape memory alloys, the following additional materials were subjected to corrosion tests: $Ni_{50}Ti_{50}$ bulk alloys, $Ni_{50}Ti_{50}$ ribbon and $Cu_{71}Zn_{25}Al_4$ ribbons.

2.2 Microstructural characterization:

The Ti-Ni-Cu ribbons melt-spun samples have been microstructurally characterized using a Tescan Vega LM Scanning Electron Microscope (SEM) equipped with a Bruker Quantax 200 EDX system with Peltier-cooled XFlash 410M silicon drift detector. SEM was used to examine the as-cast samples, before and after immersion in NaCl solution for the estimation of the corrosion effects. X-ray diffraction in a Bruker AXS D5005 diffractometer using Cu Kα radiation and differential scanning callorimetry (DSC) was carried out to identify the presence of the martensitic structure and phase transformation. The shape change on heating and on cooling was also observed macroscopically.

2.3 Solutions and experimental conditions

The electrochemical corrosion tests have been performed in 0.9% NaCl solution prepared by dissolving 9 gm of pure NaCl in one liter of bidistilled water. The samples were immersed in NaCl for 15 minutes before the measurements. All experiments were performed at the room temperature (25^o C) versus Ag/AgCl as a reference electrode.

2.4. Testing

2.4.1 Electrochemical impedance spectroscopy:

The corrosion behavior of the previous SMAs specimens was monitored using electrochemical impedance spectroscopy (EIS) technique after 15 minutes of immersion in 0.9% NaCl solution open to air and at room temperature (25° C).

A three-electrode set-up was used with impedance spectra being recorded at the corrosion potential E_{Corr}. A silver/silver chloride electrode was used as the reference electrode. It was coupled capacitively to a Pt wire to reduce the phase shift at high frequencies. EIS was performed between 0.01 Hz - 65 kHz frequency range using a frequency response analyzer (Autolab PGSTAT 30, Eco-Chemie, The Netherlands). The amplitude of the sinusoidal voltage signal was 10 mV.

2.4.2 Cyclic Voltammetery

Cyclic voltammetery measurements of specimens previously immersed for 15 minutes in 0.9% NaCl solution were made according to ASTM F746 standard test at a scan rate of 0.07 mV/sec using an Autolab PGSTAT 30 galvanostat/ potentiostat, The Netherlands. This technique was used as another screening test to evaluate the previous alloys with respect to their resistance to localized corrosion (pitting or crevice) in 0.9% NaCl solution. During this test an abrupt "electrochemical damage" is achieved by applying a wide potential range. The potential was recorded starting from a cathodic potential (about -1.75V/Ag/AgCl) and be allowed to sweep to the anodic potential direction till it reaches the pitting potential. At that potential, a sudden shift in the current to the active direction will be observed. At the pitting potential, the sample will be enforced to sweep again in the cathodic direction. The exposed surface area was 4 cm^2. All curves were normalized to 1cm^2.

3. RESULTS AND DISCUSSION

The Ni-Ti-Cu shape memory alloy ribbons in the analyzed compositional range are expected to show a phase transformation above room temperature, between the low temperature martensite (M) and the high temperature Austenite (A).

3.1. Structural analysis of the as cast ribbons

X-ray diffraction spectra of the Ti-Ni-Cu ribbons at room temperature (Fig. 1) shows strong peaks of the orthorhombic martensite and weak peaks of the B2 austenite, indicating that the sample is mostly in martensitic state and with a strong texture developed during the meltspinning process. The bump in the XRD spectra as well as a broadness of the peaks is also an indication that the sample is not fully crystalline due to the particularities of the meltspinning process involving high cooling rates. This assumption is further strengthened by the broad peaks observed in the DSC curves recorded on heating

and on cooling (Fig. 2). Both the phase transitions on heating (i.e. M→A) and on cooling (i.e. A→M) expand over a large temperature range, around 60°C strongly indicating – in conjunction 3with the x-ray data and the particularities of the meltspinning process – the presence of a partially crystalline microstructure.

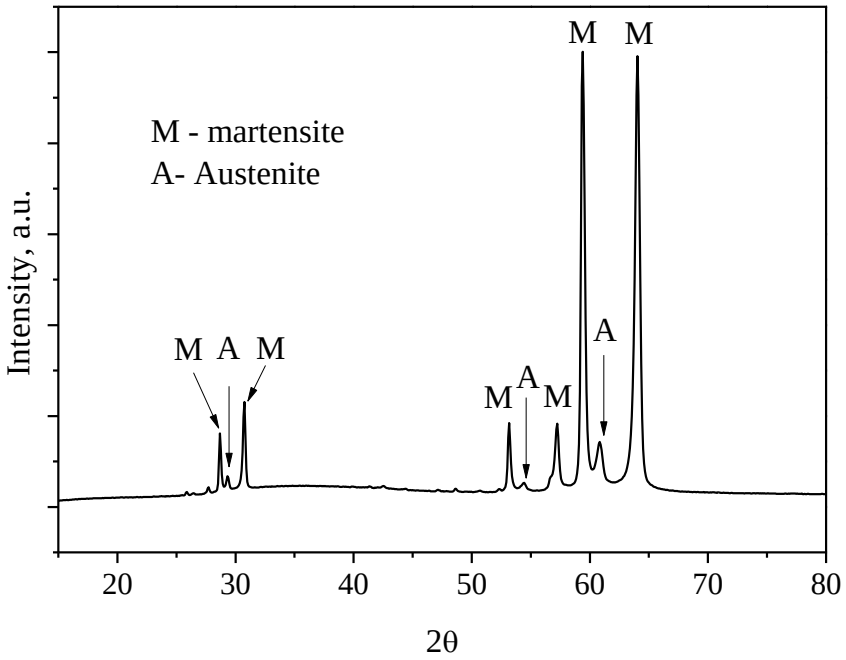

Figure 1. X-ray diffraction spectrum of the Ti-Ni-Cu ribbons

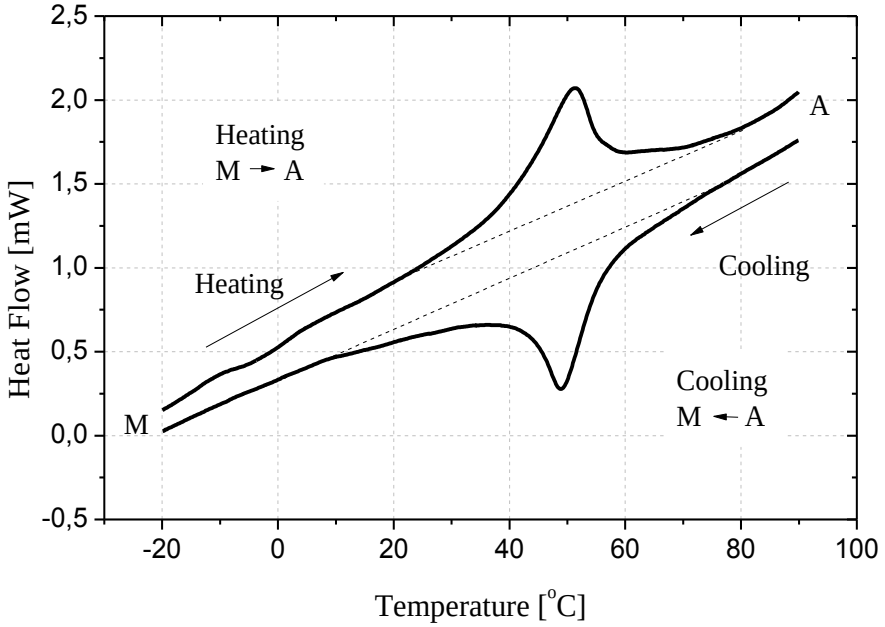

Figure 2. DSC spectra revealing the phase transformation in the Ti-Ni-Cu ribbons

3.2 Microstructural observation of corrosion effects

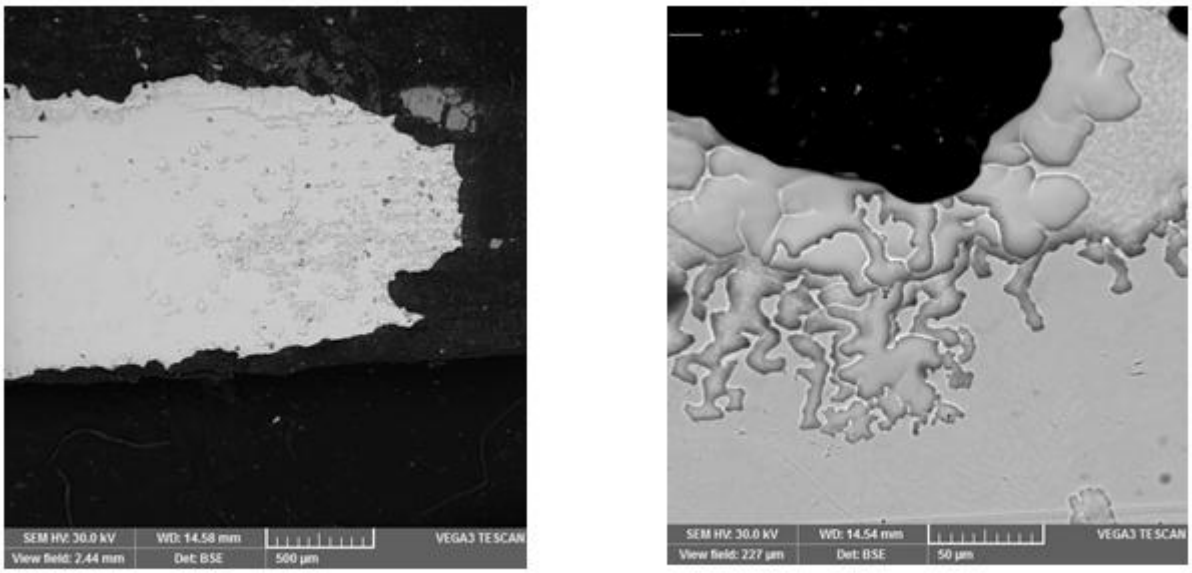

a. view of a heavily corroded end of ribbon b. details of corrosion figures

Figure 3. SEM of the shiny surface of the ribbon after corrosion test

The as-spun Ti-Ni-Cu shape memory alloy ribbons show particular surface features related to the manufacturing process. The surface of the resulting ribbon can be fine, with a shiny or rough aspect, depending on the position with respect to the copper drum during meltspinning. This surface appears to be further related to the corrosion process as it results from figs. 3 and 4.

Figure 3 shows the typical surface of the shiny side of the ribbon and the corresponding corrosion effects on the surface. By contrast, the analysis of the rough surface reveals a much more intense corrosion compared to the one observed on the shiny surface.

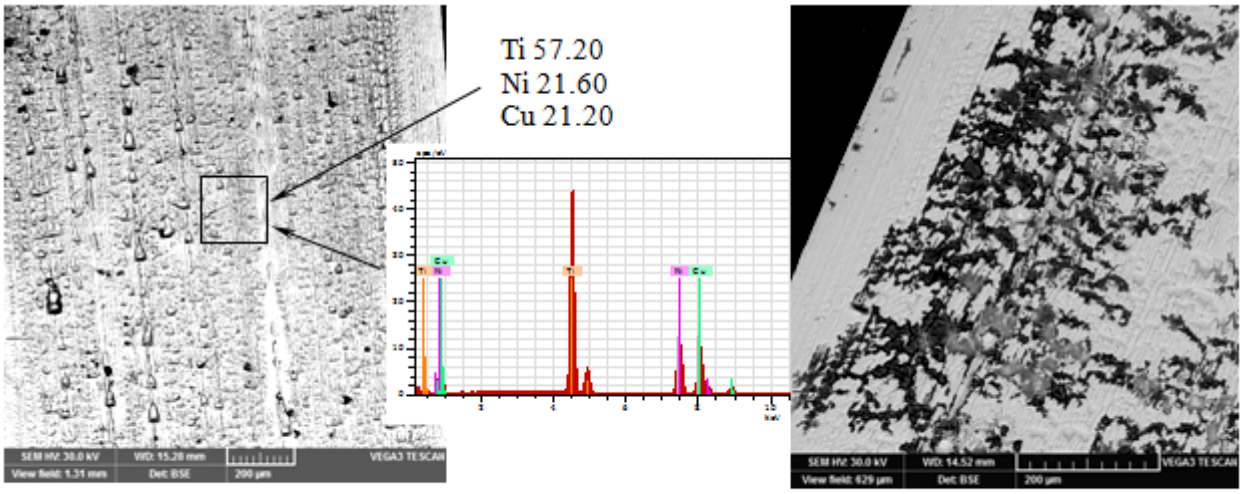

a. as spun rough face b. corroded surface of rough face

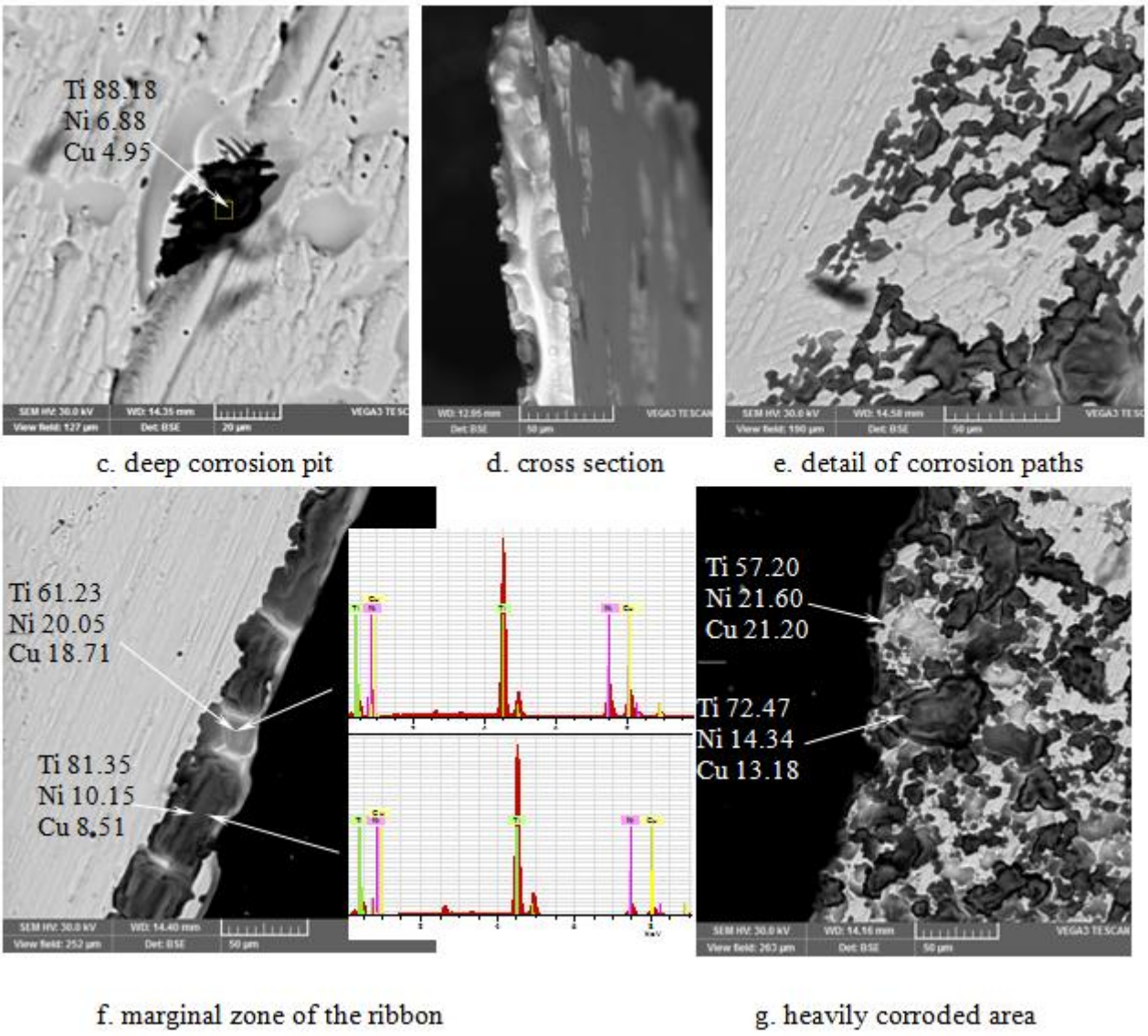

Figure 4. Microstructural details of the rough surface of the Ti-Ni-Cu ribbons before and after corrosion tests

According to the EDX measurements, the typical rough surface observed before the corrosion attack (fig 4a) has a composition of 57.20 Ti, 21.60 Ni and 21.20 Cu [at%]. Pitting effect lead to an accelerated depletion of Ni and Cu (fig. 4c) and - in the heavily corroded areas - the corrosion develops from both surfaces, although with different intensities (fig. 4d). The progress of the corrosion appears to be favored by the surface features, as it can be observed in fig. 4e.

The surface of the rough side showed solidification contours which can explain the enhancement of corrosion of the rough surface compared to the shiny one. Regardless of the intensity of the corrosion, the depletion in Ni and Cu appears consistent in all corroded areas of the sample (figs. 4f and 4g). These observations are further supported by the surface analysis of the depth profile in fig. 5 reveling the smoothness of the shiny surface compared to the rough one.

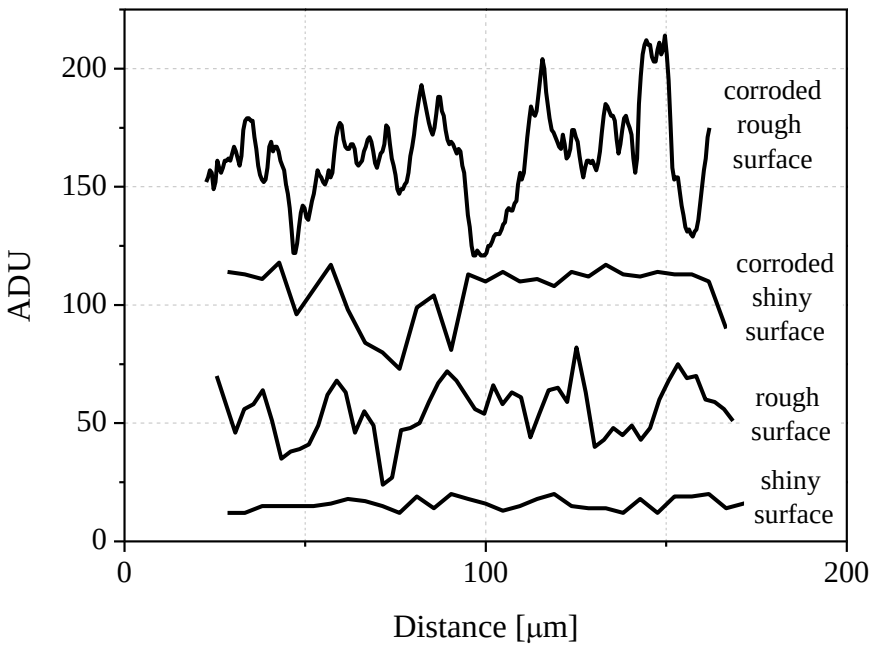

Figure 5. Microstructural details of the fine surface of the Ti-Ni-Cu ribbons before and after corrosion tests

The penetration effects on the rough surface appear up to three times more severe than the ones that resulted in the smooth surface. This result suggests that a preferential side for corrosion exists in ribbons that result with dissimilar surfaces out of the meltspinning process, i.e. ejected with only one surface in contact with the copper drum, while the opposite surface solidifies freely. The corrosion resistance appears to be significantly reduced with the decrease of the surface homogeneity since the passive film that usually form on the surface [28] looses the continuity and becomes inhomogeneous, favoring localized (pitting and crevice) corrosion. The cooling rate across the thickness of rapid solidified ribbons is higher for the surface in contact with the copper disk and the resulting structural features are influenced by this difference [29]. The crystallinity of the sample is also expected to be influenced by the variation of the cooling rate. Rough surfaces that result during the rapid solidification process on the free surface of the ribbons (i.e. solidified at lower cooling rate, thus closer to the crystalline state) favor the corrosion process, compared to the fine ones that are obtained on the surface in contact with the copper disk (where the cooling rate was higher and favorable for partial amorphization).

3.3. Electrochemical Impedance Spectroscopy (EIS)

EIS has been successfully applied to the study of corrosion systems and been proven to be an accurate method for measuring corrosion rates especially for coatings and thin films. An important advantage of EIS over other techniques is the possibility of using very small amplitude signals without significantly disturbing the properties being measured. To make an EIS measurement, a small amplitude signal is applied to a specimen over a range of frequencies.

The expression for impedance is composed of a real and an imaginary part. If the real part is plotted on the Z axis and the imaginary part on the Y axis of a chart, we get a "Nyquist plot". However, Nyquist plots have one major shortcoming. When you look at any data point on the plot, you cannot tell what frequency was used to record that point.

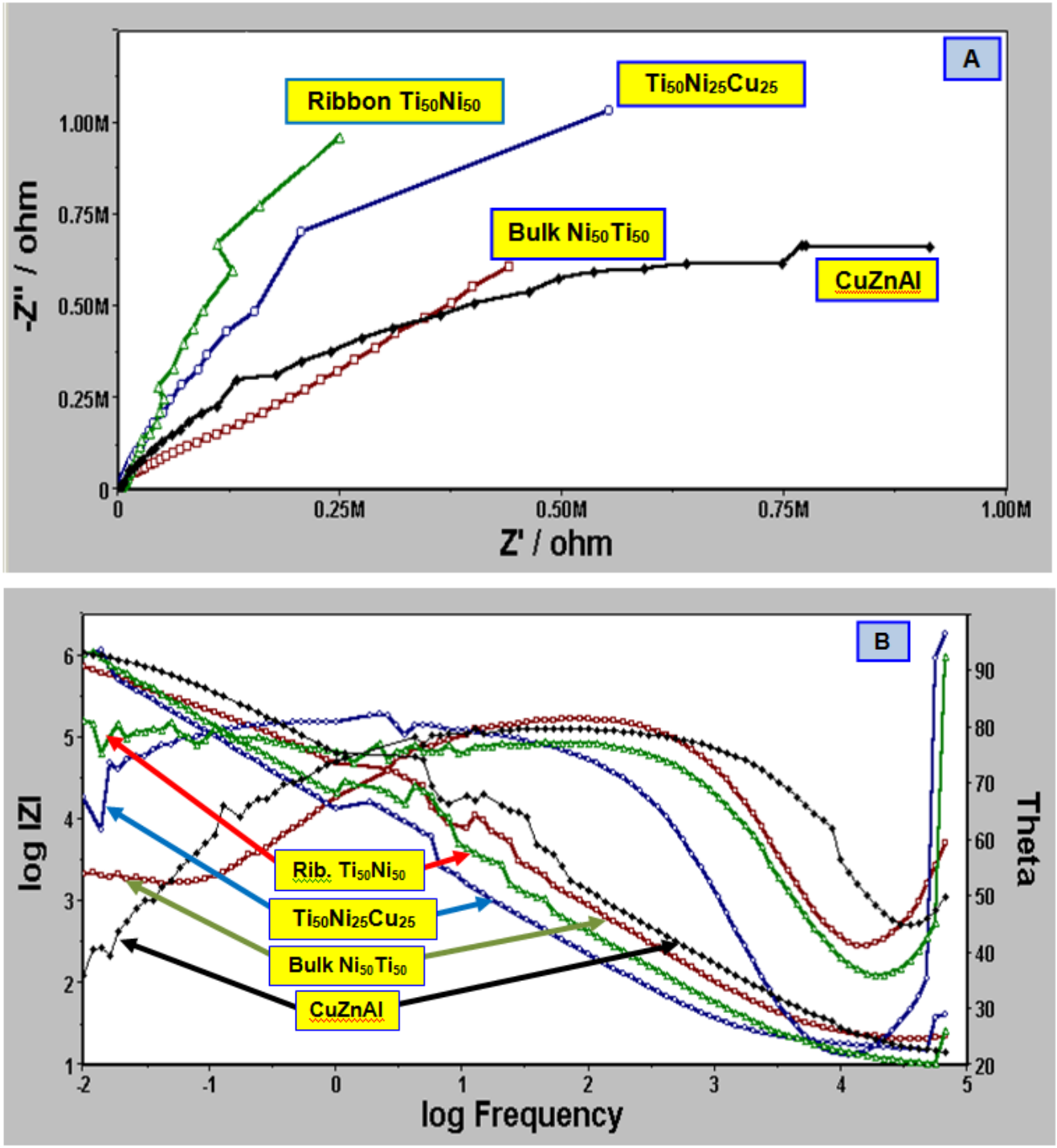

Figure 6. Electrochemical Impedance Spectroscopy Nyquist (a) and Bode (b) plots after 15 min of immersion in corrosive 0.9 NaCl solution

Therefore other impedance plots such as Bode plots are important to make a correct interpretation. In Bode plots, the impedance is plotted with log frequency on the x-axis and both the absolute value of the impedance (|Z| =Z0) and phase-shift on the y-axis. Unlike the Nyquist plot, the Bode plot explicitly shows frequency information.

In this work, Nyquist and Bode plots have been used to evaluate the corrosion resistance after immersion in NaCl solution. According to the EIS results (Figs 6a and b), and visual inspection, the ribbon samples of $Ti_{50}Ni_{50}$ and $Ti_{50}Ni_{25}Cu_{25}$ showed the best corrosion resistance of about 1.1 X 10^6 $\Omega.cm^2$. The bulk $Ti_{50}Ni_{50}$ samples showed a limited surface resistance of about 0.6 X 10^6 $\Omega.cm^2$. The improved corrosion resistance of the $Ti_{50}Ni_{25}Cu_{25}$ and $Ti_{50}Ni_{50}$ ribbon samples was confirmed by the relaxation of the impedance spectra. However, $Ti_{50}Ni_{50}$ showed a better relaxation (and hence better resistance to localized corrosion) than $Ti_{50}Ni_{25}Cu_{25}$ as shown in Fig.6a and b. According to Nyquist plots (Fig. 6a), the surface resistance of bulk $Ti_{50}Ni_{50}$ and CuZnAl is almost half (~0.6X10^6 $\Omega.cm^2$) the resistance of $Ti_{50}Ni_{25}Cu_{25}$ and $Ti_{50}Ni_{50}$ ribbon samples. The main reason behind the poor corrosion performance of bulk $Ti_{50}Ni_{50}$, and hence, limited biocompatibility is the releasing of Ni ions from Ni-Ti surface in chloride solution. Accordingly, it can be concluded that the ribbons offer much better corrosion resistance than the bulk structure due to the crystal structure in bulk compared with amorphous phase in the ribbons. Moreover, the presence of copper partially decreased the pitting corrosion resistance of Ni-Ti ribbons.

Bode plots (Fig. 6b) provided further explanation to support these results. The bulk $Ti_{50}Ni_{50}$ and CuZnAl samples showed dramatic decrease of the impedance in the capacitive region, which is characteristic for the pitting process. In addition, the phase angle (θ) tended toward zero at low frequencies, indicating that the resistance of the barrier layer was being approached. An additional maximum of θ was observed for the above mentioned samples, as evident in Fig. 6b. These changes of the spectra at very low frequencies indicated the occurrence of pitting and were in agreement with visual, optical and SEM inspection. On the other hand, $Ti_{50}Ni_{50}$ and $Ti_{50}Ni_{25}Cu_{25}$ ribbon samples showed stable impedance behavior after 15 minutes of immersion in 0.9% NaCl solution. However, the stability of impedance to corrosion of $Ti_{50}Ni_{50}$ is higher than $Ti_{50}Ni_{25}Cu_{25}$.

3.4. Cyclic Voltammetery

Cyclic voltammetery technique (Figure 7) was used to evaluate the pitting corrosion resistance for the previously mentioned SMAs after 15 minutes of immersion in 0.9% NaCl solution. The potential was recorded starting from a cathodic potential and be allowed to sweep to the anodic potential direction till it reaches the pitting potential. At that potential, a sudden shift in the current to the active direction will be observed. At the pitting potential, the sample will be enforced to sweep again in the cathodic direction. The materials of the superior pitting corrosion resistance will be those that will show no loop. The less pitting corrosion resistance samples will show intersection of the returned curve with the initial curve in either anodic or cathodic branch. If the intersection will be done at the anodic branch, the potential at the point of intersection is called the protection potential, $E_{protection}$. The difference between the $E_{protection}$ - E_{corr} will represent the perfect passivity domain. At that

domain, the materials will be completely safe from pitting corrosion. And, the area under the loop will represent the chance of pitting corrosion to occur. The smaller the area is under the loop, the lower the chance for pitting corrosion to occur.

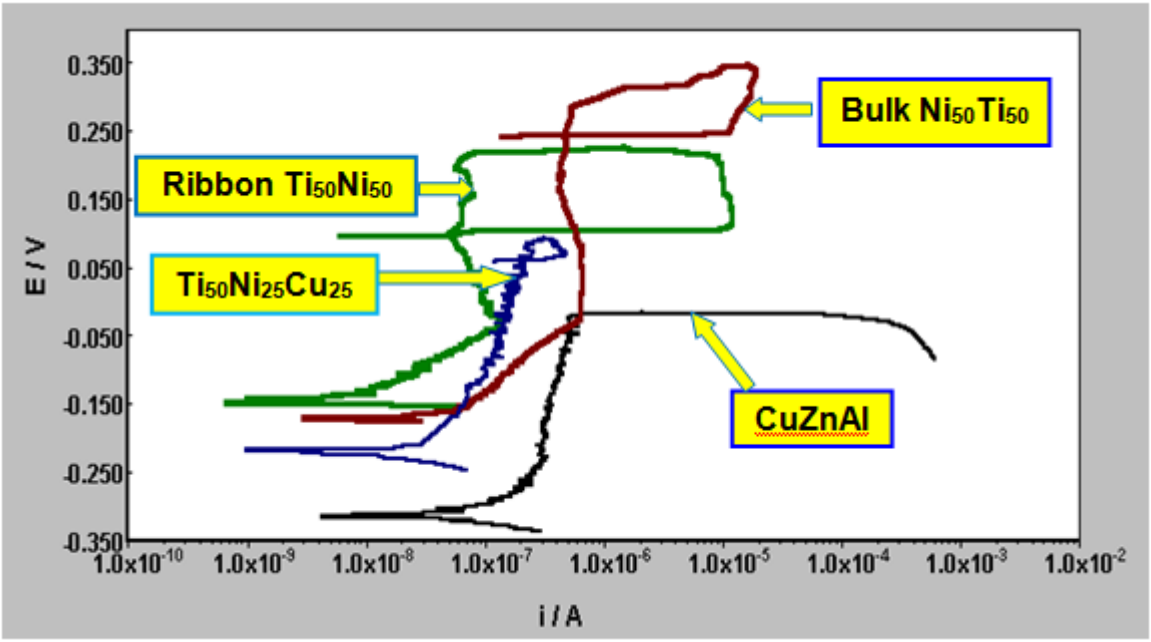

Figure 7. Cyclic voltammetery after 15 min of immersion in corrosive 0.9 NaCl solution

If the intersection will be done at the cathodic branch, the sample will have no ability to resist pitting corrosion. Moreover, pitting corrosion, in this case, can be done even under free corrosion potential. However, the smaller the area is under the loop, the lower the chance for pitting corrosion to occur. Accordingly, the sample, in this case, will have no perfect passivity domain.

The area under the loop expresses the chance for pitting corrosion to occur. The bigger the area is under the loop, the higher the chance for pitting corrosion to occur. The smallest pitting area was observed for the $Ti_{50}Ni_{25}Cu_{25}$ ribbon. Results showed that the chance for pitting corrosion to occur can be sorted in this order $Ti_{50}Ni_{25}Cu_{25}$ << $Ti_{50}Ni_{50}$ ribbon < bulk $Ti_{50}Ni_{50}$ < CuZnAl.

The apparent disagreement between the results of EIS and polarization regarding the resistance of $Ti_{50}Ni_{25}Cu_{25}$ and $Ti_{50}Ni_{50}$ can be explained as follows

1. The resistance measured by EIS is the total surface resistance i.e. pitting corrosion, general corrosion, crevice corrosion. etc. Apparently, the most predominate corrosion species in $Ti_{50}Ni_{50}$ ribbons is the diffusion of Ni from the matrix causing pitting corrosion as confirmed by other authors (26-28). Conversely, the most predominate corrosion form in $Ti_{50}Ni_{25}Cu_{25}$ is general corrosion with some few pitting. The sharp depletion of Cu content as confirmed from Fig. 4 confirmed the dissolution of copper from the surface (general corrosion).

2. The passivity domain of $Ti_{50}Ni_{50}$ and $Ti_{50}Ni_{25}Cu_{25}$ ribbons samples are about 170-150 mV respectively compared with a zero passive domain for CuZnAl. CuZnAl samples showed no resistance to pitting corrosion and the pitting corrosion can even be occurred at the open circuit potential.

3. Taking the bulk Ti_{50}-Ni_{50} samples as a base, the passive current of ribbon $Ti_{50}Ni_{50}$ is higher than $Ti_{50}Ni_{25}Cu_{25}$ and is 140-100 times respectively lower than for bulk $Ti_{50}Ni_{50}$ samples.

4. Bulk $Ti_{50}Ni_{50}$, ribbon $Ti_{50}Ni_{50}$ and $Ti_{50}Ni_{25}Cu_{25}$ samples showed passivity domain of about 150-170 mV compared with a zero passive domain for CuZnAl samples.

5. The passive current of $Ti_{50}Ni_{50}$ ribbon samples is 40 μA more passive than the $Ti_{50}Ni_{25}Cu_{25}$ and; the pitting potential of $Ti_{50}Ni_{50}$ ribbon samples is 140 mV more passive than the $Ti_{50}Ni_{25}Cu_{25}$. Such results confirm the better corrosion resistance of $Ti_{50}Ni_{50}$. Therefore, the passive layer formed on $Ti_{50}Ni_{25}Cu_{25}$ ribbon samples behaves as barrier to protect the material substrate from the reaction with dissolved oxygen in NaCl solution and hence impedes the localized corrosion.

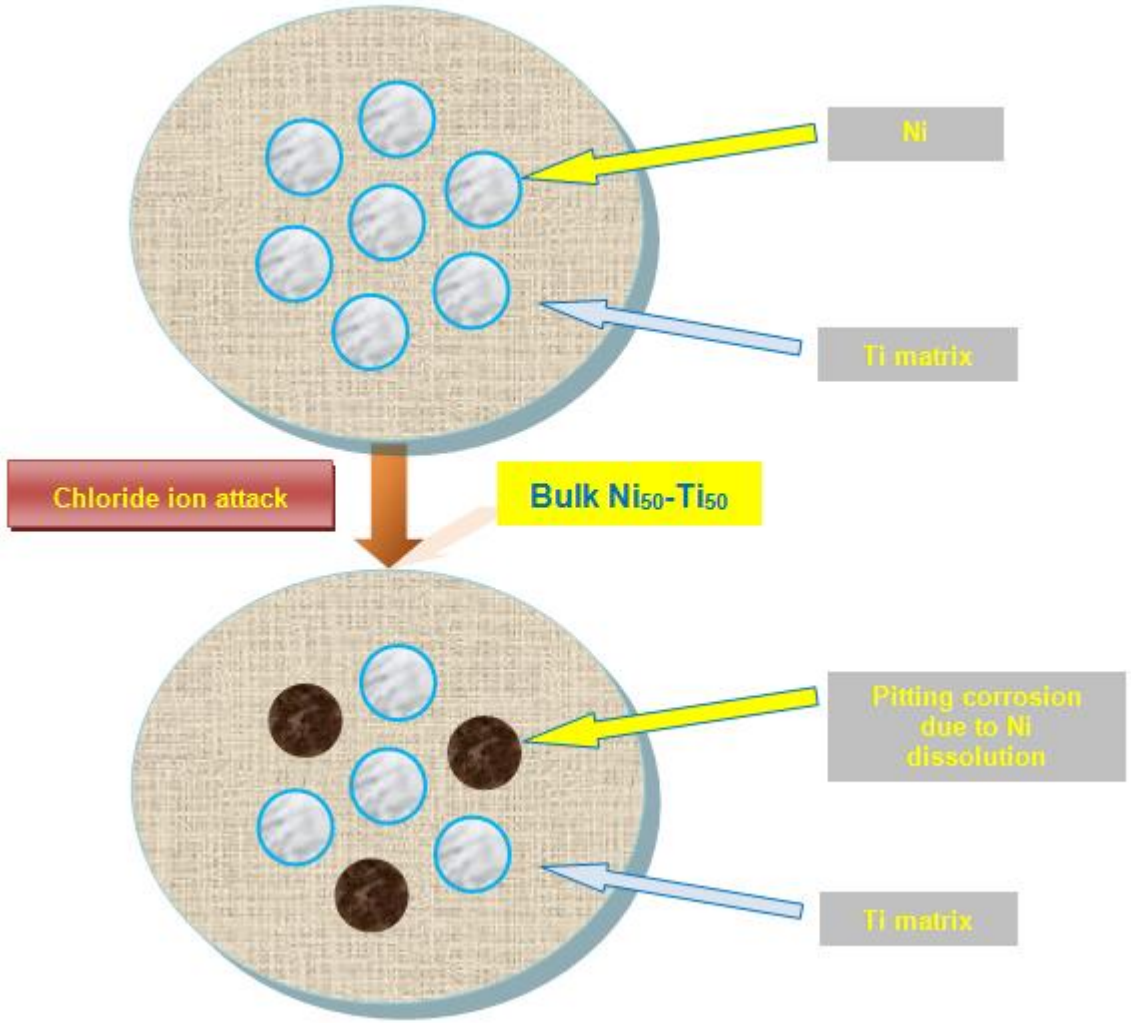

Figure 8. schematic representation (not to scale) showing the proposed mechanism of corrosion for Bulk Ni_{50}-Ti_{50} in chloride solution (increased pitting corrosion attack)

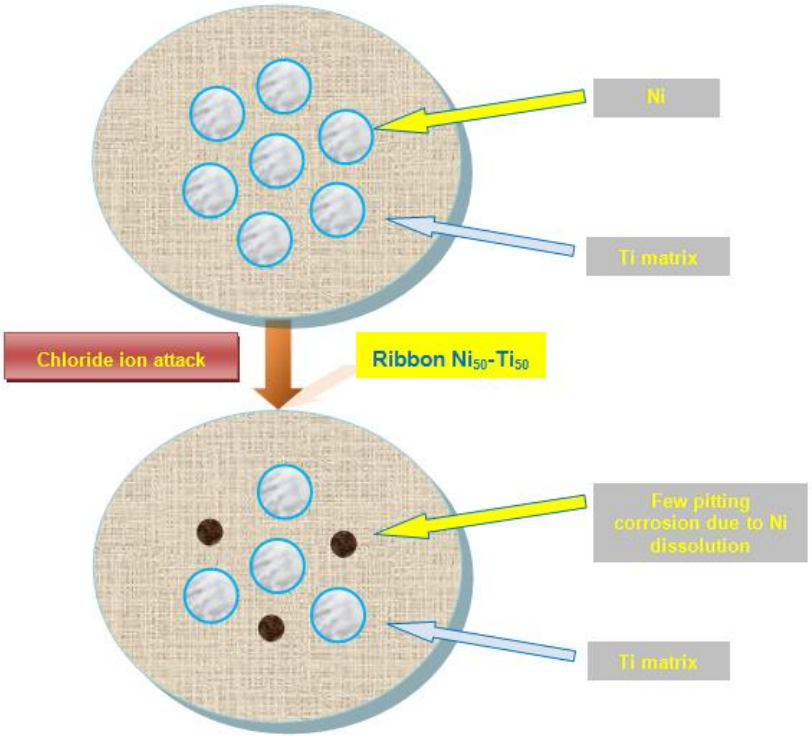

Figure 9. schematic representation (not to scale) showing the proposed mechanism of corrosion for Ribbon Ni_{50}-Ti_{50} in chloride solution (Improved pitting corrosion resistance)

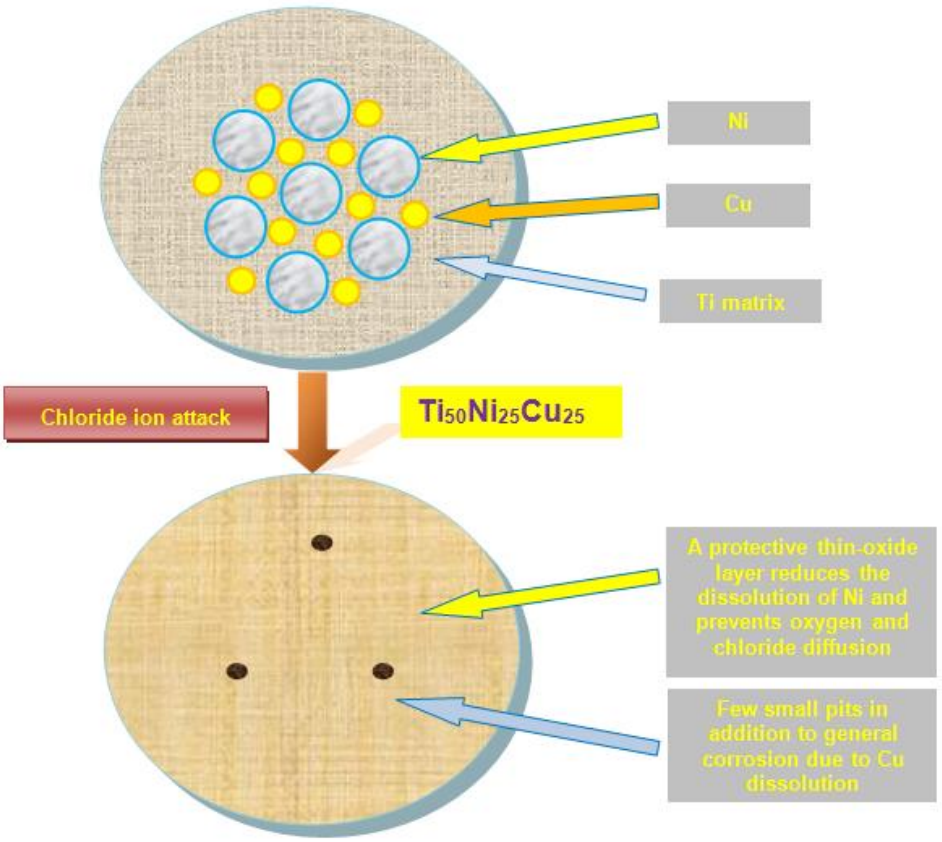

Figure 10. schematic representation (not to scale) showing the proposed mechanism of corrosion for Ti_{50}-Ni_{25}-Cu_{25} in chloride solution

The schematic representations in Figs 8-10 summarize the film formation in each material and the chance of occurrence of pitting or general corrosion. It is important to notice the occurrence of general corrosion in Ni-Ti-Cu as a predominant corrosion form compared with more pitting susceptibility in Ti-Ni substrate. These results confirm the previous results that copper plays an important role in the corrosion protection process by forming Cu-rich oxide film acts as a barrier to oxygen diffusion to the metal surface thereby impeding the localized corrosion but not preventing the dissolution of surface copper from Ni-Ti-Cu ribbons.

4. CONCLUSIONS

1. The corrosion behavior of partially crystalline Ni-Ti-Cu ribbons manufactured by meltspinning has been investigated using electrochemical impedance spectroscopy (EIS) and cyclic voltammetry techniques in 0.9% NaCl solution.

2. The corrosion of the Ti-Ni-Cu ribbons appears to be significantly influenced by the surface quality of the ribbons. Rough surfaces that result during the rapid solidification process on the free surface of the ribbons favor the corrosion process, compared to the fine ones that are obtained on the surface in contact with the copper disk, where the cooling rate is the highest.

3. The overall corrosion resistance of partially crystalline Ni-Ti ribbons is better than Ni-Ti-Cu ribbons. However, it was evidenced the presence of copper as an alloying element plays an important role in improving the resistance to pitting corrosion by forming Cu-rich oxide film that acts as a barrier to oxygen diffusion to the metal surface thereby impeding the diffusion of Ni from the matrix. However, such Cu-rich surface film cannot not prevent the dissolution of surface copper from Ni-Ti-Cu ribbons and therefore, severe general corrosion was detected.

ACKNOWLEDGEMENTS
The support of the Romanian National Authority for Scientific Research, grant CNCS – UEFISCDI, project number PN-II-ID-PCE-2011-3-0837 is acknowledged.

References

1. K. Asami, B. P. Zhang, M. Mahmood, H. Habazaki, K. Hashimoto, *Scr. Mater*. 4 (2001) 1655–1658
2. X. Li, Y. Wang, C. Du, B. Yan, *J Nanosci Nanotechnol.* 10, 11 (2010) 7226-7230
3. T. N. Kim, A. Balakrishnan, B. C. Lee, W. S. Kim, K. Smetana, J. K. Park, B. B. Paniggrahi, *Biomed. Mater.* 2 (2007) S117–S120
4. J. J. Oak, D. V. Louzguine-Luzgin, A. Inoue, *Mater. Sci. Eng*., C 29 (2009) 322–327
5. W. R. Osório, , A. Cremasco, P. N. Andrade, A. Garcia, R. Caram, *Electrochim. Acta*, 55 (2010) 759–770
6. J. Fornell, N. Van Steenberge, A. Varea, E. Rossinyol, E. Pellicer, S. Suriñach, M.D. Baró, J. Sort, *J. Mech. Behavior of Biomedical Mat*., 4 (2011) 1709–1717
7. A. S. Svetlana, *Bio-Medical Materials and Engineering*, 12 (2002) 69–109

8. Y.-F. Zheng, B.B. Zhang, B.L. Wang, Y.B. Wang, L. Li, Q.B. Yang, L.S. Cui, *Acta Biomaterialia*, , 7 (2011) 2758–2767
9. Y.-F Zheng, Q. Y. Wang, L. Li, J. Biomedical Mat. Res. Part B: *Applied Biomaterials*, 86B (2007) 335–340, 200
10. Y. Furuya, H. Kimura, M. Matsumoto, T. Matsumoto, *Trans. Mater. Res. Soc*. Japan, B18 (1993) 1033–1036
11. S. Miyazaki, K. Komatsubara, K. Otsuka, *Collected Abstracts of Annual Fall Meeting of Japan Institute of Metals*, Sapporo (1998) 408
12. A.V. Shelyakov, N.N. Sitnikov, V.V. Koledov, D.S. Kuchin, A.I. Irzhak, N.Yu. Tabachkova, *Int. J. Smart and Nano Materials*, 2:2 (2011) 68-77
13. C.M. Craciunescu, J. Li, M. Wuttig, *Thin Solid Films*, 434 (2003) 271-275
14. Y.Q. Fu, J.K. Luo, A.J. Flewitt, S.E. Ong, S. Zhang, H.J. Du, W.I. Milne, *Smart Mater. Struct*., 16 (2007) 2651-2657
15. Y. Liu, *Mater. Sci. Eng. A*, 35 (2003) 4286–4291
16. H. Rosner, A V. Shelyakov, A M. Glezer, K. Feit, P. Schloßmacher, *Mater. Sci. Eng*. A, 273–275 (1999) 733–737
17. X. Wen, N. Hang, X. Li, Z. Gao, *Biomed. Mat. Eng*., 7 (1997) 1
18. P. Schloßmacher, H. Rosner, A.V. Shelyakov, A. M. Glezer, *Mater. Sci. Forum*, 327/328 (2000) 131–134
19. N. Resnina, S. Belyaev, A. Shelyakov, *Eur. Phys. J. Special Topics*, 158 (2008) 21-26
20. T. Nam, S. Park, T. Kim, Y. Kim, *Smart Mater. Struct*. 14 (2005) S239–S244
21. J. Morgiel, E. Cesari, J. Pons, A. Pasko, J. J. Dutkiwicz, *Mat. Sci*., 375 (2002) 319–325
22. H. Rumpf, C. M. Crăciunescu, H. Modrow, Kh. Olimov, E. Quandt, M. Wuttig, *J. Magn. and Magn. Mater*., 302, 22 (2006) 421-428
23. G. Rondelli, B. Vicentini, *Biomaterials*, 23, 3 (2002) 639-644
24. O. W. Bertacchini, D. C. Lagoudas, E. Patoor, *Int. J. Fatigue*, 31/10 (2009) 1571–1578
25. L. Chenghao, S. Hongyan, *Rare Metal Materials and Engineering*, (2001) *2*.
26. E. Kassab, L. Neelakantan, M. Frotscher, S. Swaminathan, B. Maaß, M. Rohwerder, J. Gomes, G. Eggeler, *Mater Corros.*,10 (2012), doi: 10.1002/maco.201206587.
27. Du Hejun, S. Zhang, Jack K. Luo, A. J. Flewitt, I. M. William, Biopsy applications of Ti50Ni41Cu9 shape memory films for wireless capsule endoscope, Proc. SPIE 5648, Smart Materials III, 2004, 184
28. B. Clarke, W. Carroll, Y. Rochev, M. Hynes, D. Bradley, D. Plumley, *J Biomed Mater Res A* (2006) 79A, 61–70.
29. M. Takezawa, K. Aiba, H. Yasuda, Y. Morimoto, T. Hidaka, J. Yamasaki, H. Kato, M. Yagi, *J. Magnetism and Magnetic Materials*, 2007, 310/2, 3, 2572–2574.